

Efficient Domain Generalization in Wireless Networks with Scarce Multi-Modal Data

Minsu Kim, Walid Saad *Fellow, IEEE*, and Doru Calin

Abstract—In 6G wireless networks, multi-modal machine learning (ML) models can be leveraged to enable situation-aware network decisions in dynamic environments. However, trained ML models often fail to generalize under domain shifts when training and test data distributions are different because they often focus on modality-specific spurious features. In practical wireless systems, domain shifts occur frequently due to dynamic channel statistics, moving obstacles, or hardware configuration. To mitigate domain shifts, one can do extensive measurement or generate synthetic multi-modal data from various wireless environments. However, without access to target domains, this approach is highly time-consuming. Moreover, public multi-modal wireless datasets are extremely scarce unlike vision or language tasks. Thus, there is a need for learning frameworks that can achieve robust generalization under scarce multi-modal data in wireless networks. In this paper, a novel and data-efficient two-phase learning framework is proposed to improve generalization performance in unseen and unfamiliar wireless environments with minimal amount of multi-modal data. In the first stage, a physics-based loss function is employed to enable each base station (BS) to learn the physics underlying its wireless environment captured by multi-modal data. The data-efficiency of the physics-based loss function is analytically investigated. In the second stage, collaborative domain adaptation is proposed to leverage the wireless environment knowledge of multiple BSs to guide under-performing BSs under domain shift. Specifically, domain-similarity-aware model aggregation is proposed to utilize the knowledge of BSs that experienced similar domains. To validate the proposed framework, a new dataset generation framework is developed by integrating CARLA and MATLAB-based mmWave channel modeling to predict mmWave received signal strength from LiDAR, RGB, radar, and GPS. Simulation results show that the proposed physics-based training requires only 13% of data samples to achieve the same performance as a state-of-the-art baseline that does not use physics-based training. Moreover, the proposed collaborative domain adaptation needs only 25% of data samples and 20% of FLOPs to achieve the convergence compared to baselines.

I. INTRODUCTION

Next-generation wireless systems such as 6G can potentially leverage a broad range of sensing modalities, including LiDAR, RGB, radar, or GPS, so as to provide situational awareness [1]. For instance, in vehicular networks, multi-modal sensing data can be exploited for various communication functions, such as beam forming and blockage prediction [2]. Multi-modal sensing data can also be used for learning dynamic wireless environments such as path loss and received signal strength (RSS) estimation [3]. To process multi-modal

M. Kim and W. Saad are with the Institute for Advanced Computing, Virginia Tech, Alexandria, VA, USA (email: {msukim, walids}@vt.edu).

D. Calin is with MediaTek, Warren, NJ, USA (email: {doru.calin@mediatek.com}).

The implementation code will be available on <https://github.com/news-vt>. A preliminary version of this work was submitted to IEEE International Conference on Communications (ICC) 2026.

data, machine learning (ML) models are widely adopted because neural networks can extract and fuse features from different modalities. Hence, fusing heterogeneous information sources can provide a wireless network with situational-awareness, such as moving blockages, obstacles, or trajectories that single-modality ML schemes cannot fully provide under wireless environments.

Despite the potential benefits of using multi-modal data, conventional data-driven training methods (e.g. supervised or semi-supervised) require a significant amount of data. However, multi-modal wireless communications scenarios have typically scarce datasets compared to other ML tasks such as vision and language. For instance, DeepSense 6G [4] has around one million data samples while LAION-5B [5] has around five billion data samples. Hence, models often become overfitted to modality-specific spurious features such as noise, camera brightness, or LiDAR intensity patterns [6] due to training data scarcity. Hence, trained multi-modal models often fail to generalize to unseen environments when training and test data distributions are different [7]. Such a data distribution change after training is called *domain shift*. In practical wireless environments, domain shifts can happen frequently due to inherently dynamic channel statistics, blockages, weather, and device-related characteristics. For example, consider a millimeter wave (mmWave) beamforming task that should be performed based on multi-modal data input in vehicular scenarios as done in [2]. Environmental change can affect each modality sensor. For example, a target vehicle with unfamiliar shape can appear while rain or snow can reduce the intensity of LiDAR and attenuate radar signals. Such domain shifts induce a change to the input distribution of the ML model, and they are defined as *covariate shift*. Meanwhile, large vehicles can block the mmWave signal of the target vehicle, removing line-of-sight (LoS) paths. A target vehicle can have different mmWave antenna position on the roof or the windshield, changing the optimal beam indices completely. Such domain shifts are known as *concept shift*, and they change the mapping between the input and output (i.e., beam index). Both covariate and concept shifts can significantly affect the performance of ML models trained by conventional data-driven methods because learned mappings do not align with the new distributions. One can collect a sufficient amount of data from every possible wireless environment to mitigate domain shifts, but this approach is not practical. Without access to target domains, robust generalization requires extensive measurement or synthetic data generation, which is costly. Therefore, there is a need to design new learning frameworks that can achieve robust generalization with minimal multi-modal data in wireless networks.

A. Related Works

There are a handful of works [8]–[13] that considered the problem of ML generalization for wireless communication scenarios. In [8], the authors proposed a two-stage multi-modal pre-training and downstream task adaptation framework to utilize one universal model for diverse downstream tasks. The work in [9] used a large language model (LLM) to integrate language and radio frequency modalities to fine-tune it for diverse tasks. In [10], the authors proposed an analogical learning framework to allow a model to learn the scenario-related information that can be used across different scenarios. However, the works in [8]–[10] considered the generalization of a pre-trained model to different tasks rather than generalization to domain shifts caused by dynamic wireless environments. The authors in [11] and [12] considered generalization for gesture classification using wireless sensing under different subcarriers and scattering environments. In [13], the authors proposed a model for radio frequency fingerprinting to identify transmitters to generalize over various receivers. However, the works in [11]–[13] only considered covariate shifts, while concept shifts are not studied. In practice, both domain shifts can occur frequently in wireless environments, and their generalization performance can be limited only under covariate shifts. Moreover, the works in [11]–[13] assumed access to multiple training data domains, which does not always hold in practice due to data scarcity.

Meanwhile, the works in [14]–[17] used wireless models such as channel propagation as a prior physical information to improve the data efficiency. In [14], the authors used the geometry of indoor maps to predict RSS by diving receivers into LoS and non-line-of-sight (NLoS). The authors in [15] proposed physics-informed reinforcement learning for mmWave indoor navigation tasks with digital twins. The work in [16] proposed an imaged-based wireless propagation based model based on generative adversarial networks to predict the RSS of cells. In [17], the authors used a 3GPP path loss formula for indoor RSS prediction for LoS receivers while used regression based methods for NLoS. However, the solutions in [14]–[17] did not consider the robustness of their trained models to domain shifts caused by wireless environments. Moreover, the works in [14]–[17] also did not analyze the impact of using prior physical information during training on the data-efficiency. To the best of our knowledge, there are no current works that jointly consider multiple modalities, domain generalization, and data efficiency to mitigate domain shifts in wireless communication scenarios.

B. Contributions

The main contribution of this paper is a novel data-efficient ML framework that can promptly achieve robust domain generalization to unseen and unfamiliar wireless environments with minimal multi-modal data. The proposed framework consists of two phases: In the first phase, we train each base station (BS)’s model by exploiting the channel propagation physics of the wireless environment captured by multi-modal input. Specifically, we propose to use a physics-based loss function to mitigate domain shifts and to improve data-efficiency. We

theoretically prove how the physics-based loss function can improve data efficiency by regularizing the hypothesis space. In the second phase, we propose collaborative domain adaptation, which utilize multiple BSs’ knowledge of their wireless environment to help a BS under domain shifts. Specifically, we first propose a method to measure the domain similarity between two BS. Then, we propose domain-similarity-aware model aggregation to use the knowledge of other BSs who experienced similar domains to adapt to domain shifts with minimal amount of data. To validate the proposed framework, we develop a new dataset generation framework, which predicts mmWave RSS using multi-modal sensor (LiDAR, RGB, Radar, and GPS) inputs in urban vehicular scenarios. We integrate CARLA [18] and MATLAB for the data generation. Specifically, we use CARLA’s autonomous vehicle functions to induce dynamic blockages and multi-modal sensing modules. Based on the generated CARLA environment, we use MATLAB to perform ray-tracing to calculate the RSS of the coverage area of BSs. Simulation results show that our proposed framework can achieve significantly more robust generalization and data efficiency compared to the standard fine-tuning and state-of-the-art baselines that used physics-prior information. Specifically, our framework requires only 13% of the training data to achieve the same performance as the baseline that does not use physics-based training. For the proposed collaborative domain adaptation, our method needs only 25% of data samples and 20% of floating point operations (FLOPs) to converge compared to baselines while the standard fine-tuning fails to converge due to lack of data.

The rest of this paper is organized as follows. Section II presents the system model. In Section IV, we present a use case to validate the proposed idea. Section V provides the data generation framework. In Section VI, simulation results are provided. Finally, conclusions are drawn in Section VII.

II. SYSTEM MODEL

We consider K BSs equipped with a uniform planar array (UPA) of U antennas and a set \mathcal{V} of V vehicles distributed over a given geographical area. We assume that each BS is equipped with multi-modal sensors including camera, LiDAR, radar, and GPS. Based on a captured multi-modal input \mathbf{X}_k , BS k it makes a network decision \mathbf{Y}_k . Without loss of generality, output \mathbf{Y} can be a beamforming index, channel estimation, handover decision, or RSS prediction of the surrounding area [2], [4], [8], [9]. To process multi-modal input \mathbf{X}_k , each BS k uses an ML model θ_k . In our system, a *domain* is essentially a joint probability distribution $\mathbb{P}(\mathbf{X}, \mathbf{Y})$ between input \mathbf{X} and output \mathbf{Y} . Particularly, we define the joint probability distributions $\mathbb{P}_k^{\text{train}}(\mathbf{X}, \mathbf{Y})$ and $\mathbb{P}_k^{\text{test}}(\mathbf{X}, \mathbf{Y})$ as the domain of training and test data, respectively. We define domain shift as any event that causes $\mathbb{P}_k^{\text{test}}(\mathbf{X}, \mathbf{Y}) \neq \mathbb{P}_k^{\text{train}}(\mathbf{X}, \mathbf{Y})$. Specifically, a *covariate shift* changes input distribution as $\mathbb{P}_k^{\text{train}}(\mathbf{X}) \neq \mathbb{P}_k^{\text{test}}(\mathbf{X})$, and a *concept shift* changes the mapping between \mathbf{X}_k and \mathbf{Y}_k as $\mathbb{P}_k^{\text{train}}(\mathbf{Y}|\mathbf{X}) \neq \mathbb{P}_k^{\text{test}}(\mathbf{Y}|\mathbf{X})$. In a wireless system, both covariate and concept shifts occur frequently. For example, consider a mmWave beamforming task based on multimodal input \mathbf{X} . Covariate shifts can occur

if a target vehicle has a new shape, affecting the vision domain, or under weather changes. Concept shifts can, for example, occur when a mmWave antenna is mounted in a different position on the target vehicle, changing the optimal beam index. For a mmWave RSS prediction task, unseen blockages change channel propagation paths significantly, making a new mapping between \mathbf{X} and \mathbf{Y} . Under such domain shifts, trained models often show severe performance degradation.

Although collecting additional training data can mitigate domain shifts, such an approach is prohibitively time-consuming and costly. Moreover, under domain shifts, a trained model must also be adapted within a few epochs using significantly limited of data from target domains. Hence, there is a need to design a data-efficient multi-modal training and adaptation frameworks to achieve robust generalization to unseen wireless environments.

A. Problem Formulation

Given our model, we now formulate two multi-objective optimization problems for training and adaptation, respectively. For training, we aim to minimize the amount of training data m_k^{tr} and θ_k that can optimize the generalization error under unseen domain $\mathbb{P}_k^{\text{test}}(\mathbf{X}, \mathbf{Y})$ for BS k , $\forall k$ as follows:

$$\min_{m_k^{\text{tr}}} \quad \left(m_k^{\text{tr}}, \mathbb{E}_{(\mathbf{X}, \mathbf{Y}) \sim \mathbb{P}_k^{\text{test}}(\mathbf{X}, \mathbf{Y})} [l(\mathbf{Y}, \theta_k(\mathbf{X}))] \right) \quad (1a)$$

$$\text{s.t.} \quad \theta = \arg \min_{\theta} \frac{1}{m_k^{\text{tr}}} \sum_{i=1}^{m_k^{\text{tr}}} l(\mathbf{Y}_i, \theta(\mathbf{X}_i)) \quad (1b)$$

$$(\mathbf{Y}_i, \mathbf{X}_i) \sim \mathbb{P}_k^{\text{train}}(\mathbf{X}, \mathbf{Y}), \forall i, \quad (1c)$$

where $l(\cdot)$ is a loss function. Here, $\mathbb{P}_k^{\text{test}}(\mathbf{X}, \mathbf{Y})$ can be any unseen domain, such as different antenna positions on target vehicles, unfamiliar blockage patterns, or weather changes. This problem is challenging because we need to jointly minimize m_k^{tr} and the generalization error $l(\mathbf{Y}, \theta(\mathbf{X}))$ without access to $\mathbb{P}_k^{\text{test}}(\mathbf{X}, \mathbf{Y})$. After training, we need to adapt the trained model when domain shifts occur to recover the performance. Hence, for the adaption, we aim to find optimal adapted model $\tilde{\theta}_k$ and minimal amount of data m_k^{te} from $\mathbb{P}_k^{\text{test}}(\mathbf{X}, \mathbf{Y})$ to minimize the generalization error as follows:

$$\min_{m_k^{\text{te}}, \tilde{\theta}_k^{(E)}} \quad \left(m_k^{\text{te}}, \mathbb{E}_{(\mathbf{X}, \mathbf{Y}) \sim \mathbb{P}_k^{\text{test}}(\mathbf{X}, \mathbf{Y})} [l(\mathbf{Y}, \tilde{\theta}_k^{(E)}(\mathbf{X}))] \right) \quad (2a)$$

$$\text{s.t.} \quad \tilde{\theta}_k^{(0)} \in \Theta'_k = \{\theta_k : \theta_k \text{ that satisfies (1b)}\} \quad (2b)$$

$$\tilde{\theta}_k^{(e+1)} = \tilde{\theta}_k^{(e)} - \eta \nabla_{\tilde{\theta}_k} \left(\frac{1}{m_k^{\text{te}}} \sum_{i=1}^{m_k^{\text{te}}} l(\mathbf{Y}_i, \tilde{\theta}_k^{(e)}(\mathbf{X}_i)) \right) \quad (2c)$$

$$(\mathbf{Y}_i, \mathbf{X}_i) \sim \mathbb{P}_k^{\text{test}}(\mathbf{X}, \mathbf{Y}), \forall i; e \in [0, E-1], \quad (2d)$$

where E is the number of epochs for adaptation. This problem is challenging since the amount of available data from $\mathbb{P}_k^{\text{test}}(\mathbf{X}, \mathbf{Y})$ is significantly smaller than $\mathbb{P}_k^{\text{train}}(\mathbf{X}, \mathbf{Y})$. Next, we present how to solve problems (1a) and (2a) with the proposed physics-based training and collaborative domain adaptation.

III. PROPOSED PHYSICS-BASED TRAINING AND COLLABORATIVE ADAPTATION

To solve problems (1a) and (2a), we design a two-phase learning framework. For the first phase, we make predictions of a model consistent with channel propagation so as to embed domain-invariant physical knowledge into the training for (1a). For the second phase, we use the knowledge of other trained BSs to help under-performing BSs under domain shifts based on domain similarity for (2a).

A. Physics-based Training

In the first phase, we solve problem (1a) to minimize the generalization error with minimal training data. Essentially, without access to $\mathbb{P}_k^{\text{test}}(\mathbf{X}, \mathbf{Y})$, model θ_k usually overfits to $\mathbb{P}_k^{\text{train}}(\mathbf{X}, \mathbf{Y})$, thereby being susceptible to covariate and concept shifts. Model θ_k usually memorizes noise in $\mathbb{P}_k^{\text{train}}(\mathbf{X}, \mathbf{Y})$ rather than learning the relationship between \mathbf{X} and \mathbf{Y} . To mitigate this, we make predictions of model θ_k consistent with channel propagation in the wireless environment of BS k . As such, model θ_k can be robust to covariate and concept shifts because its predictions are based on physical laws invariant over domains. To this end, we use a physics-based loss function to embed channel propagation characteristics into the training, as follows:

$$\mathcal{L}_{\text{total}}(\mathbf{Y}_k, \theta_k(\mathbf{X}_k)) = \mathcal{L}_{\text{data}}(\mathbf{Y}_k, \theta_k(\mathbf{X}_k)) + \lambda \mathcal{L}_{\text{phy}}(\mathbf{Y}_k, \theta_k(\mathbf{X}_k)), \quad (3)$$

where $(\mathbf{X}_k, \mathbf{Y}_k) \sim \mathbb{P}_k^{\text{train}}(\mathbf{X}, \mathbf{Y})$, \mathbf{Y}_k is a ground truth output (e.g., beamforming index or RSS), $\mathcal{L}_{\text{data}}(\mathbf{Y}_k^{\text{true}}, \theta_k(\mathbf{X}_k)) = \frac{1}{C} \sum_{i=1}^C l_{\text{data}}(\mathbf{Y}_{k,i}, \theta_k(\mathbf{X}_{k,i}))$ is an empirical loss function with batch size C , and l_{data} is a supervised loss function such as mean square error (MSE) or mean absolute error (MAE). Similarly, $\mathcal{L}_{\text{phy}}(\mathbf{Y}_k, \theta_k(\mathbf{X}_k)) = \frac{1}{C} \sum_{i=1}^C l_{\text{phy}}(\mathbf{Y}_{k,i}, \theta_k(\mathbf{X}_{k,i}))$, $l_{\text{phy}}(\mathbf{Y}_{k,i}, \theta_k(\mathbf{X}_{k,i}))$ is a physics-based loss function, and λ is the corresponding coefficient. Here, \mathcal{L}_{phy} penalizes the model if its predictions do not follow the physical law of the channel propagation. Hence, \mathcal{L}_{phy} can reduce the possible search space of θ_k , improving data efficiency. To formalize this intuition, we first define a hypothesis class Θ_k of θ_k . Without loss of generality, we assume l_{data} and $l_{\text{phy}} \in [0, 1]$ as done in [19], [20]¹. To simplify the notation, we drop index k hereinafter. For given $\tau \in [0, 1]$ and a certain domain $\mathbb{P}(\mathbf{X}, \mathbf{Y})$, we define $\Theta(\tau)$ as the subset of hypothesis Θ as follows

$$\Theta(\tau) = \{\theta \in \Theta : \bar{\mathcal{L}}_{\text{phy}}(\mathbf{Y}, \theta(\mathbf{X})) \leq \tau\}, \quad (4)$$

where $\bar{\mathcal{L}}_{\text{phy}}(\mathbf{Y}, \theta(\mathbf{X})) = \mathbb{E}_{(\mathbf{X}, \mathbf{Y}) \sim \mathbb{P}(\mathbf{X}, \mathbf{Y})} [\mathcal{L}_{\text{phy}}(\mathbf{Y}, \theta(\mathbf{X}))]$ is the expected loss function. In the following theorem, we derive the impact of the physics-based loss function $\bar{\mathcal{L}}_{\text{phy}}$ on the data efficiency.

Theorem 1. Suppose $\exists \theta^* \in \Theta$ s.t. $\bar{\mathcal{L}}_{\text{data}}(\mathbf{Y}, \theta^*(\mathbf{X})) = 0$ and $\bar{\mathcal{L}}_{\text{phy}}(\mathbf{Y}, \theta^*(\mathbf{X})) = 0$. Then, $\forall \epsilon_0, \epsilon_1 \in (0, 1)$ with $\delta \in (0, 1)$, and m samples from $\mathbb{P}(\mathbf{X}, \mathbf{Y})$ are sufficient to achieve error ϵ_1 with probability $1 - \delta$, where

$$m \geq \frac{1}{\epsilon_1} \left[\ln(|\Theta(\epsilon_0)|) + \ln \frac{1}{\delta} \right] \quad (5)$$

¹In practice, we can clip gradients to limit the impact of the loss function.

Proof. See Appendix A. \square

From Theorem 1, we can see that the physics-based loss function reduces the required amount of data m to achieve error ϵ_1 . As ϵ_0 decreases, the size of $\Theta(\epsilon_0)$ decreases, leading to a smaller amount of data to achieve error ϵ_1 . Hence, \mathcal{L}_{phy} regularizes the ML model to be consistent with how channels propagate, thereby improving the data efficiency and robustness to domain shifts. Meanwhile, if we set ϵ_0 as ∞ , the size of $\Theta(\epsilon_0)$ becomes the whole possible space of Θ , resulting in more required data. Here, we note that having θ_k^* with zero loss is a theoretical limit that may not be achievable in real-world scenarios. However, Theorem 1 still shows that any θ_k that adheres to the designed \mathcal{L}_{phy} can improve the data efficiency. In addition, we corroborate our theorem in simulations as shown in Fig. 5.

B. Collaborative Domain Adaptation

In the second phase, we aim to solve problem (2a) to find the minimal amount of data from $\mathbb{P}_k^{\text{test}}(\mathbf{X}, \mathbf{Y})$ to adapt the model under domain shifts. During inference, each BS is deployed to make network decisions in real-time. If the performance of BS's model degrades due to domain shifts, it should adapt its model to the current domain, using data samples from $\mathbb{P}_k^{\text{test}}(\mathbf{X}, \mathbf{Y})$. However, the amount of available data is extremely limited during inference, and the adaptation must happen in few epochs to support the real-time inference. Hence, we propose a *collaborative domain adaptation framework*, in which BSs collaborate to guide under-performing BSs to improve the data-efficiency and adaptation speed. Essentially, if a given BS experiences a domain shift, it can request help from other BSs to retrieve their models. Then, it aggregates the received models based on similarities between the current domain and other BSs' domains. Hence, by using the knowledge of BSs who have high domain similarity, the under-performing BS can adapt to the current domain promptly with limited amount of data.

1) *Measuring Domain Similarities:* We first study how to measure the domain similarity between two BSs. The last layer of θ_k will be given by $\mathbf{v}_k \in \mathbb{R}^{N \times m}$, where N is the dimension of the network decision of θ_k and m is the dimension of feature vector $\mathbf{f} \in \mathbb{R}^m$. The output of θ_k can be given by $\mathbf{Y}_k = \langle \mathbf{f}, \mathbf{v}_k \rangle$. BS k encodes multi-modal input \mathbf{X}_k into features \mathbf{f}_k using deterministic or probabilistic mapping (e.g., dropout) with θ_k . Hence, we can know that the joint probability distribution $\mathbb{P}_k(\mathbf{X}, \mathbf{Y}, \mathbf{f})$ contains almost the same information between \mathbf{X}_k and \mathbf{Y}_k as $\mathbb{P}_k(\mathbf{X}, \mathbf{Y})$ does. As such, we consider $\mathbb{P}_k(\mathbf{X}, \mathbf{Y}, \mathbf{f})$ as a domain of BS k hereinafter.

By using Bayes rule, we have:

$$\mathbb{P}_k(\mathbf{X}, \mathbf{Y}, \mathbf{f}) = \frac{\mathbb{P}_k(\mathbf{Y}|\mathbf{f}, \mathbf{X})}{\mathbb{P}_k(\mathbf{Y}|\mathbf{X})} \times \mathbb{P}_k(\mathbf{f}|\mathbf{X}) \times \mathbb{P}_k(\mathbf{X}, \mathbf{Y}) \quad (6)$$

$$\approx \mathbb{P}_k(\mathbf{f}|\mathbf{X}) \mathbb{P}_k(\mathbf{X}) \mathbb{E}_{\mathbb{P}_k(\mathbf{f}|\mathbf{X})} [\mathbb{P}_k(\mathbf{Y}|\mathbf{f})] \quad (7)$$

$$= \mathbb{P}_k(\mathbf{f}) \mathbb{E}_{\mathbb{P}_k(\mathbf{f}|\mathbf{X})} [\mathbb{P}_k(\mathbf{Y}|\mathbf{f})] \quad (8)$$

$$\approx \mathbb{P}_k(\mathbf{f}), \quad (9)$$

where (7) follows from the fact that \mathbf{X} and \mathbf{f} provide the almost same information to \mathbf{Y} , and (9) results from the fact

Algorithm 1: The overall pipeline for the physics-based training and collaborative domain adaptation.

```

Input: Training dataset  $\{\mathbf{X}_k, \mathbf{Y}_k\}$ , and model  $\theta_k$ , and data from
unseen domain  $\mathbf{X}'_k, \forall k$ .
1 Training:
2   for each agent  $k$  with  $\{\mathbf{X}_k, \mathbf{Y}_k\}$  do
3     Update  $\theta_k$  using (3);
4 Inference:
5   for each BS  $k$  with  $\mathbf{X}'_k$  (in parallel) do
6     Calculate  $\mu_k$  and  $\Sigma_k$ ;
7     if Domain shift occurs then
8       Retrieve models of other BSs;
9       Calculate domain similarity  $\gamma$  using (10);
10      Aggregate the retrieved models using (11);
11      Adapt  $\theta_k$  using  $\mathbf{X}'_k$ ;

```

that \mathbf{Y} is deterministic for given \mathbf{f} and the last layer \mathbf{v} . From (9), we can see that a domain can be approximated as the probability distribution of the encoded multi-modal features \mathbf{f}_k . We assume that $\mathbb{P}_k(\mathbf{f})$ follows a multivariate normal distribution [21]. Each BS k tracks its domain $\mathbb{P}_k(\mathbf{X}, \mathbf{Y}, \mathbf{f})$ by calculating the mean μ_k and covariance Σ_k of $\mathbb{P}_k(\mathbf{f})$ in the current batch. We use the Wasserstein-2 distance $W(\cdot)$ to measure the similarity of the domains of two BSs as it holds symmetry and triangle inequality. Then, the similarity of the domains of two BSs can be given as

$$W(k, j) = \sqrt{\|\mu_k - \mu_j\|_2^2 + \text{Tr}(\Sigma_k + \Sigma_j - 2\sqrt{\Sigma_k^{1/2} \Sigma_j \Sigma_k^{1/2}})}. \quad (10)$$

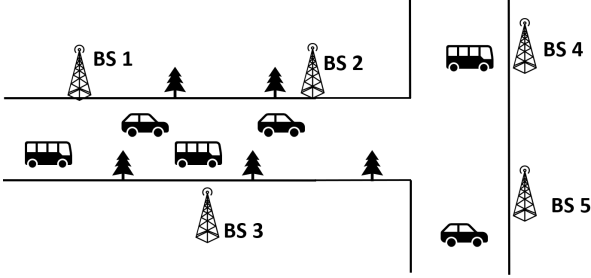
From (10), we can measure how similar their domains are. If BS k experiences an unseen domain, BSs with similar domains can have knowledge that is helpful for adapting to the current domain. Next, we present how to aggregate models of other BSs based on domain similarities.

2) *Domain Similarity Aware Aggregation:* Under domain shifts, BS k first requests help to other BSs to retrieve their model parameters $\{\theta_i\}, \forall i \neq k$. Then, BS k calculates $W(k, i), \forall i \neq k$ using the received models and data \mathbf{X}'_k from the current domain. Lastly, it generates a new model by aggregating the received models based on the measured domain similarities as follows

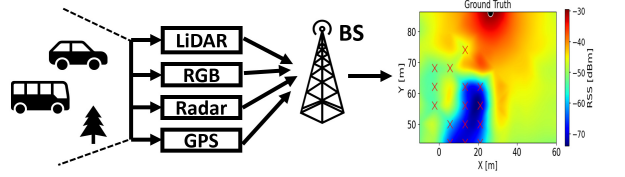
$$\theta_k \leftarrow \sum_{i \neq k} \gamma_i \theta_i, \text{ where } \gamma_i = \text{softmax} \left(\frac{1}{W(k, i)} \right). \quad (11)$$

We assign higher weights to models that show higher domain similarity with the current data samples \mathbf{X}'_k . After the aggregation, BS k adapts its model to \mathbf{X}'_k for a few epochs. This collaborative domain adaptation improves the data efficiency and adaptation speed because BS k initializes its model using other BSs' models who have high domain similarities. Hence, the proposed framework allows the adaptation with significantly limited amount of data during inference. The overall pipeline is summarized in Algorithm 1.

The proposed collaborative domain adaptation has complexity of $\mathcal{O}(K)$ because an under-performing BS needs to retrieve model parameters of other BSs and calculate domain similarities.



(a) An illustration of the use case system model.



(b) An illustration of multi-modal based RSS map prediction.

Fig. 1: An illustration of the considered use case and multi-modal based RSS prediction.

IV. USE CASE: MULTI-MODALITY BASED MMWAVE RSS PREDICTION

To validate the proposed frameworks in practical wireless networks scenarios, we present mmWave RSS prediction as a use case because it can leverage multi-modal sensors to capture surrounding objectives.

A. System Overview

We consider multi-modal sensor (camera, LiDAR, radar, GPS) based mmWave RSS map prediction in urban vehicular scenarios as shown in Fig. 1. We construct a mmWave radio environment map that can capture the dynamics of surrounding environment from multi-modal sensors. Hence, the constructed map can potentially be used to guide networking algorithms in dynamic scenarios such as resource allocation or network slicing. Based on a captured multi-modal input \mathbf{X}_k , each BS k predicts the current RSS values \mathbf{Y}_k over a set of receiver grids \mathcal{N} of $N = N_x \times N_y$ with height r_h of its coverage area using its model θ_k . The RSS of a receiver (i, j) , where $1 \leq i \leq N_x$ and $1 \leq j \leq N_y$, significantly depends on whether it has an LoS path or not. If (i, j) has an LoS path, its RSS is largely governed by the distance to the serving BS and first-order reflections [17], [22] as follows

$$R_{ij} = R_{ij}^{\text{LoS}} + R_{ij}^{\text{reflection}}, \text{ if } (i, j) \text{ has an LoS path,} \quad (12)$$

where R_{ij}^{LoS} is the RSS from a direct beam between (i, j) and the serving BS and $R_{ij}^{\text{reflection}}$ is the RSS from the reflected beams from surrounding obstacles and grounds. We model R_{ij}^{LoS} using the 3GPP-Umi LoS path loss modeling [23] as follows

$$PL_{ij}^{\text{LoS}} = 32.4 + 17.3 \log_{10}(d_{ij}) + 20 \log_{10}(f_c) + S_f, \quad (13)$$

where d_{ij} is the distance between (i, j) and its serving BS, f_c is the carrier frequency normalized by the unit of GHz, and S_f is the shadowing factor. Then, R_{ij}^{LoS} can be given as

$$R_{ij}^{\text{LoS}} = P_{\text{tx}} + G_{\text{tx}} + G_{\text{rx}} - PL_{ij}^{\text{LoS}}, \quad (14)$$

where P_{tx} is the transmission power and G_{tx} and G_{rx} are the directional transmit and receiver antenna gains, respectively. If there is no LoS path, the RSS of (i, j) will be highly dependent on the location of the receiver and the attenuation

and diffraction values of blockages. Hence, for the NLoS case, we model the RSS as R_{ij}^{LoS} attenuated by blockages:

$$R_{ij} = R_{ij}^{\text{LoS}} - R_{ij}^{\text{blockage}}, \text{ if } (i, j) \text{ has no LoS path,} \quad (15)$$

where R_{ij}^{blockage} is the attenuated RSS due to blockage.

We assume that each BS knows the position of vehicles in its coverage area as estimated by basic safety messages broadcast by the vehicles [24]. Next, we apply the physics-based training to the proposed use case.

B. Physics-Based Training

We first specify the $\mathcal{L}_{\text{total}}$ term as defined in (3). For $\mathcal{L}_{\text{data}}(\mathbf{Y}_k, \theta_k(\mathbf{X}_k))$, we use an MSE loss function between predicted RSS and true RSS as $\mathcal{L}_{\text{data}}(\mathbf{Y}_k, \theta_k(\mathbf{X}_k)) = \frac{1}{N} \sum_{(i,j) \in \mathcal{N}} (\hat{R}_{k,ij} - R_{k,ij})^2$. For $\mathcal{L}_{\text{phy}}(\mathbf{Y}_k, \theta_k(\mathbf{X}_k))$, we divide it into the case when receiver (i, j) , $1 \leq i \leq N_x$ and $1 \leq j \leq N_y$ has a LoS path or only has NLoS paths. We design $\mathcal{L}_{\text{LoS}}(\theta_k(\mathbf{X}_k))$ to align the predictions of θ_k with the physical law of LoS scenarios as follows:

$$\mathcal{L}_{\text{LoS}}(\theta_k(\mathbf{X}_k)) = \frac{1}{|\mathcal{N}_{\text{LoS}}|} \sum_{(i,j) \in \mathcal{N}_{\text{LoS}}} \left[R_{k,ij}^{\text{blockage}} + \max(0, R_{k,ij}^{\text{reflection}} - \bar{R}_{k,ij}) \right], \quad (16)$$

where \mathcal{N}_{LoS} is a set of receivers that have a LoS path and $\bar{R}_{k,ij}$ is the bound of reflection gain $R_{k,ij}^{\text{reflection}}$. Intuitively, for receivers with LoS paths, the RSS reduction term $R_{k,ij}^{\text{blockage}}$ should be minimized as there should be no blockage. We use a hinge loss $\max(0, R_{k,ij}^{\text{reflection}} - \bar{R}_{k,ij})$ to penalize too large RSS gains from reflections. Here, $\bar{R}_{k,ij}$ is also a predicted value to bound $R_{k,ij}^{\text{reflection}}$ based on the captured multi-modal input \mathbf{X}_k on the location of receiver (i, j) . Similarly, we define $\mathcal{L}_{\text{NLoS}}(\theta_k(\mathbf{X}_k))$ to allow θ_k to learn the channel propagation of NLoS cases as follows

$$\mathcal{L}_{\text{NLoS}}(\theta_k(\mathbf{X}_k)) = \frac{1}{|\mathcal{N}_{\text{NLoS}}|} \sum_{(i,j) \in \mathcal{N}_{\text{NLoS}}} \left[R_{k,ij}^{\text{reflection}} + \max(0, B_{k,ij} - R_{k,ij}^{\text{blockage}}) \right], \quad (17)$$

where $\mathcal{N}_{\text{NLoS}}$ is a set of receivers that only have NLoS paths and $B_{k,ij}$ is the bound of the RSS reduction from blockages $R_{k,ij}^{\text{blockage}}$. We minimize $R_{k,ij}^{\text{reflection}}$ to penalize large reflection

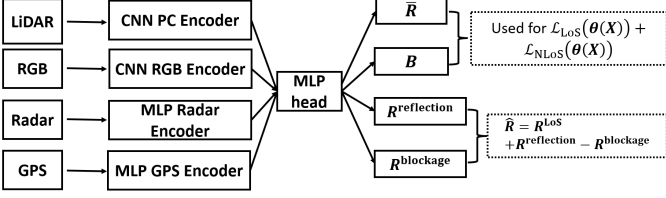


Fig. 2: An illustration of the multi-modal model architecture.

gains for receivers in \mathcal{N}_{LoS} . For mmWave signals, blockages often decrease RSS significantly. Hence, we train $B_{k,ij}$ to penalize too small RSS attenuation in \mathcal{N}_{LoS} . Note that $B_{k,ij}$ is also a predicted value based on \mathbf{X} . The labels of \mathcal{N}_{LoS} and $\mathcal{N}_{\text{NLoS}}$ are available from ray-tracing results when generating ground-truth RSS. We provide more detailed information on how we generate realistic datasets in Sec. V.

Now, we present the architecture of our ML model in Fig. 2 to process multi-modal input \mathbf{X} . The designed ML outputs $\hat{R}_{k,ij}$, $\bar{R}_{k,ij}$, and $B_{k,ij}$ for $\forall k \in \mathcal{K}$ and $\forall (i, j), 1 \leq i \leq N_x$ and $1 \leq j \leq N_y$. To capture unique pattern in each modality, we design the corresponding encoders to process raw modality data. We utilize a small convolutional neural network (CNN) encoder for RGB inputs. For LiDAR, we first project point clouds into 2D dimension with bird's-eye view and use a CNN encoder to extract transformed 3D features. We use the highest point sampling to pre-process radar inputs and encode them with multilayer perceptron (MLP) layers. Similarly, an MLP encoder is used to process GPS inputs since they are low dimension vectors. We provide more detail about the pre-processing in Section. VI. We concatenate the output of each encoder and forward it to the MLP head for the fusion. The MLP head predicts values $R_{k,ij}^{\text{reflection}}$, $R_{k,ij}^{\text{blockage}}$, $\bar{R}_{k,ij}$, and $B_{k,ij}$, $\forall (i, j), 1 \leq i \leq N_x$ and $1 \leq j \leq N_y$, using the shared encoded output from each encoder. We use all the predicted values during the training to calculate the physics-guided losses (16) and (17). After training, each BS k predicts $\hat{R}_{k,ij} = R_{k,ij}^{\text{LoS}} + R_{k,ij}^{\text{reflection}} - R_{k,ij}^{\text{blockage}}$ discarding $\bar{R}_{k,ij}$ and $B_{k,ij}$. More detailed information of the pre-processing of each modality data and architecture is provided in Sec. VI.

As described in Sec. III-B, after training, each BS k tracks the statistics of μ_k and Σ_k under its current domain. If BS k experiences a domain shift, it requests help from other agents to retrieve their models. Here, the communication overhead is negligible because of the throughput of typical backhauls of BSs. For instance, the throughput of V-band can up to 10 Gbps [25]. Subsequently, it measures the domain similarities of other BSs and aggregates their models based on (11). Then, it adapts its model to the new samples for a few epochs. Next, we present how to generate multi-modal training data for the mmWave RSS prediction.

V. MULTI-MODAL DATASET GENERATION FOR MMWAVE RSS PREDICTION

To validate the idea of the proposed framework with the use case, we need a multi-modal dataset that can induce covariate/concept shifts to multiple BSs in dynamic wireless

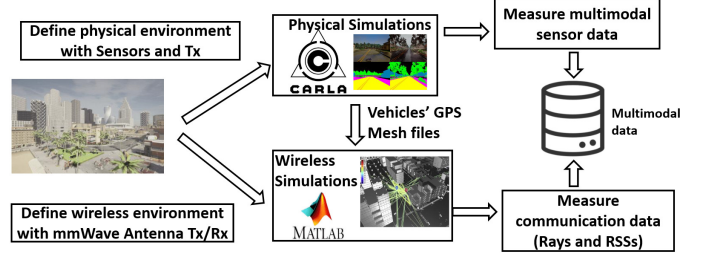


Fig. 3: An illustration of the multi-modal simulation framework based on CARLA and MATLAB.

environments. To the best of our knowledge, there is no such public dataset for multi-modal mmWave RSS prediction. We now present a multi-modal simulation framework to generate our training data. Our data generation framework is based on [2], which predicts mmWave beamforming vectors, with the following changes. Firstly, we change the task as mmWave RSS prediction in the surrounding area of BSs. We also include multiple BSs for collaborative domain adaptation to tackle domain shifts. Meanwhile, [2] is used for a single BS without considering domain shifts.

The workflow of our simulation framework is illustrated in Fig. 3. We use the autonomous vehicular simulator CARLA [18] to generate multi-modal sensing information and a virtual urban environment. Based on the generated urban environment and vehicles, we use MATLAB to do wireless communication experiments. Our framework has four main steps: CARLA environment setup, multi-modal sensing data generation, map reconstruction, and wireless communication experiments based on the generated environments. We integrate CARLA's multi-modal sensing ability and vehicular simulations into MATLAB's communication toolboxes. This approach provides flexibility to make domain shifts to vehicular environments in CARLA and to see their impact on wireless environments in MATLAB.

1) *CARLA Environment Setup*: We generate multiple vehicles and BSs within the CARLA environment. We use CARLA's traffic control and navigation functions for autonomous movements of vehicles and traffic rules. Our environment setup enables dynamic blockage patterns and multi-modal sensing conditions to generate various domain shifts.

- *BS placements*: We place BSs at fixed points as roadside units.
- *Vehicle placements*: We spawn vehicles in random locations around the generated BSs. Spawned vehicles follow pre-defined traffic rules and speed limits.
- *Environmental dynamics*: We control brightness and traffic density to simulate different covariate and concept shifts (e.g., day/night or heavier traffic).

2) *Generating Multi-modal Sensing Data*: At each BS, we instantiate the following sensor modalities:

- An RGB camera that captures the current frame to provide visual context such as blockage detection and object classification.
- A LiDAR sensor that provides distance, object shape, and blocked region in 3D point clouds.

- A radar that measures distance and velocity information of surrounding objects.
- A GPS that records vehicle coordinates and velocities.

Based on multi-modal data, the BSs can capture the details of dynamic environments such as movements of vehicles, surrounding obstacles, and buildings. We synchronize all sensing data in a time frame.

3) *Map Reconstruction*: To do wireless communication experiments in MATLAB, we need to import the generated CARLA environments into MATLAB. We follow the steps in [2] to make the CARLA environments compatible with MATLAB using Blender API [26]. We first export the CARLA environment into a ply 3D file format. We then use the Blender API to script the conversion process to preserve the geometry, coordinates, and scales of the environments. The output of the Blender API is imported into MATLAB as a mesh file, which is consistent with the original CARLA environment.

4) *Wireless Communication Simulation*: We import the generated 3D environment file into MATLAB to perform ray-tracing to capture mmWave channel propagation in the current environment. We set each BS as a transmitter and locate multiple receivers over the grids of the coverage area of the BS. We trace signal paths, path loss, reflection, diffraction, and LoS existence of each receiver. The RSS of each receiver is calculated for each received ray considering reflections, scattering, and diffraction. To enable dynamic environmental change, updated vehicle locations from CARLA are used to simulate ray-tracing.

We combine the multi-modal sensor data from CARLA and the corresponding ray-tracing results including RSS and LoS labels. Specifically, our multi-modal dataset consists of:

- Multi-modal Sensor Input: RGB, LiDAR, Radar, and GPS.
- Ray-tracing Results: RSS, path loss, delay spread, angle of arrival, angle of departure, and LoS existence of each receiver.
- Time and positional information: Time frame, vehicle IDs, and coordinates of vehicles, BSs, and receivers.

We use the constructed dataset for the proposed physics-based training in Sec. III-A and collaborative domain adaptation in Sec. III-B to validate the proposed framework.

In summary, our multi-modal data generation framework integrates autonomous vehicles and wireless communication simulations. We essentially generated dynamic urban environments to capture dynamic blockage and object patterns caused by moving vehicles. Then, we imported the CARLA environments to MATLAB to do ray-tracing. Our approach captures how the dynamics of the environment affect the mmWave channel propagation. We use our multi-modal data to simulate the proposed use case in Sec. IV.

VI. SIMULATION RESULTS AND ANALYSIS

We generate our dataset using the ‘Town 10’ map in CARLA to simulate an urban environment with up to 50 vehicles. We deploy five BSs along the map. We provide the example RGB frames of BSs 1 to 4 in Fig. 4. We set a 300 ms time interval between each time frame. We

generate around 4K training datasets, 1K validation datasets called VAL-1, and another 2K validation datasets called VAL-2 for each BS. For VAL-1, we induce new traffic patterns by making unseen blockages or obstacle patterns as shown in Fig. 4b, thereby inducing covariate and concept shifts. As such, new blockage patterns induce unseen mapping between \mathbf{X} and \mathbf{Y} , and the distribution of \mathbf{X} also changes. For BSs 1, 2, and 3, we induce new obstacle patterns by placing large vehicles at different locations, leading to concept shift-dominated domain shifts. For BSs 4 and 5, we induce stronger domain shifts by generating unseen large vehicles. For VAL-2, we decrease the brightness level by 25% and inject zero mean Gaussian noises $\mathcal{N}(0, 1)$, $\mathcal{N}(0, 0.5^2)$, and $\mathcal{N}(0, 0.25^2)$ to Radar, GPS, and LiDAR input data, respectively. For VAL-2, the induced domain shifts only change the distribution of inputs $\mathbb{P}[\mathbf{X}]$ while $\mathbb{P}[\mathbf{Y}|\mathbf{X}]$ does not change. For the wireless communication simulations, we set the height of each BS to 5.5 m and $P_{tx} = 25$ dBm [27], [28]. We assume each BS is equipped with 4×4 UPA antennas. Receivers are distributed evenly over $N = 8 \times 8$ grids over 80 m \times 40 m coverage area per each BS [29] to match the field-of-view of its camera. We assume receivers have a single antenna with $r_h = 1.5$ m.

We first pre-process each modality and forward it to the corresponding encoder as follows

- *LiDAR*: We project raw LiDAR point clouds [x, y, z, intensity] onto a 2D plane. This bird’s-eye view transformation provides the locations and positions of surrounding objects while filtering out ground reflections [2]. We use four convolutional layers and one MLP layer to encode the pre-processed point clouds input.
- *Radar*: We use the highest point sampling to pre-process radar input [velocity, azimuth, altitude, depth]. Hence, we down-sample radar inputs to a fixed size. We use three MLP layers with the max-pooling to encode the pre-processed radar inputs.
- *GPS*: We record GPS inputs as a csv format. We use three MLP layers with the max-pool to encode GPS inputs.
- *RGB*: Camera images are first normalized and scaled to 256×256 resolution. We use a pre-trained ResNet-18 to encode RGB inputs.

We concatenate all the encoded modality inputs and learnable receiver embedding to differentiate each receiver. We use three MLP layers as our head for the prediction.

We first train a model of each BS using its training dataset following (3) and test on its VAL-1 and VAL-2 datasets. We average all results over five random seeds. We implement our training in PyTorch. We use 50 epochs with a batch size of 64 and set the initial learning rate as 1.0×10^{-4} with the learning rate decay at (10, 30) epochs. We set $\lambda = 0.5$ for our physics-based loss. We consider three baselines for comparison purposes. **Baseline 1** predicts RSS values directly without utilizing any physics prior information (12)-(17). As such, Baseline 1 is trained only with MSE loss, which is widely used for regression tasks [8], [29], [30]. **Baseline 2** [14] penalizes LoS and NLoS receiver points differently when calculating MSE loss function, by giving more weights to NLoS points. We scale the loss of NLoS points by 20% more.

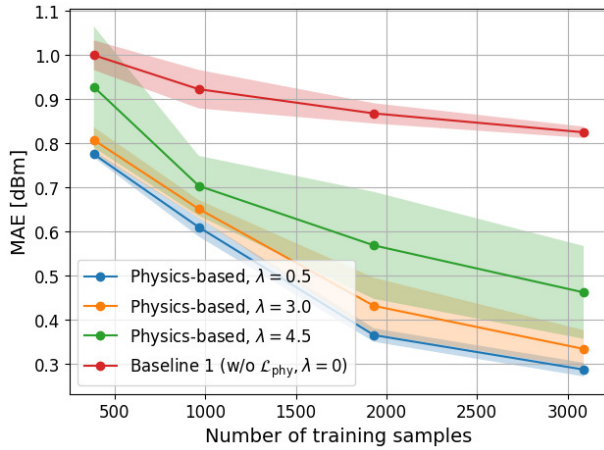


(a) Example RGB samples of BS 1 to 4 from training datasets.

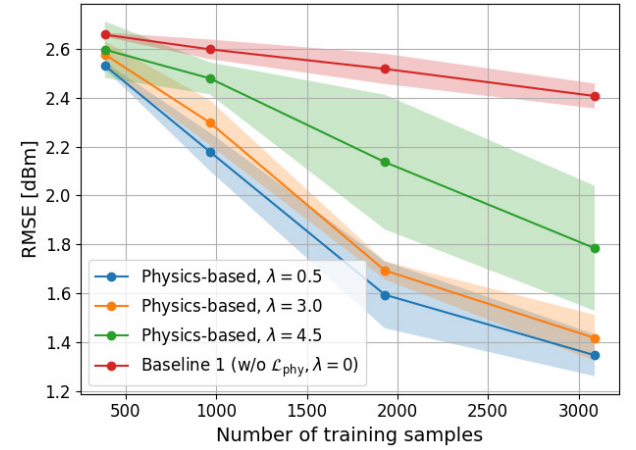


(b) Example RGB samples of BS 1 to 4 from VAL-1 datasets.

Fig. 4: Example RGB samples of BS 1, 2, 3, and 4



(a) MAE on VAL-1 with respect to the amount of training data of BS 1.



(b) RMSE on VAL-1 with respect to the amount of training data of BS 1.

Fig. 5: Performance of BS 1 with respect to the amount of training data.

Baseline 3 [17] uses 3GPP path loss formulas for RSS of LoS points while using regression for NLoS for input features. We report MAE and root mean square error (RMSE) for performance metrics.

Figure 5 shows the performance of the trained model of BS 1 for an increasing amount of training data on its VAL-1 dataset. As shown in Fig. 5a, the VAL-1 induces concept shift-dominated domain shifts due to unfamiliar blockage and obstacle patterns from the training dataset. We can see that our physics-based model outperforms Baseline 1 in terms of the generalization performance and data efficiency. For the MAE, the proposed model already achieves around 0.8 dBm of MAE with only 12.5% of the raining data used by Baseline 1. Compared to Baseline 1, our physics-based model achieves faster improvement for increasing the amount of the training data. The physics-based loss function limits the available hypothesis space to a set that follows the designed physics law during training. This reduces the possible search space, and makes model parameters generalize robustly across unseen domains. Meanwhile, as λ increases, the performance decreases since we regularize θ too strongly with \mathcal{L}_{phy} . Hence, the available search space becomes too limited for $\mathcal{L}_{\text{data}}$, leading

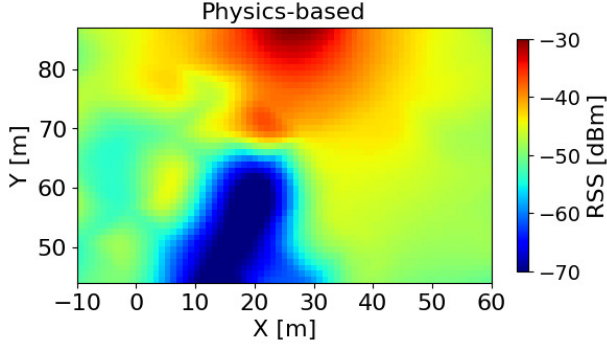
to sub-optimal performance. Therefore, Figure 5 corroborates Theorem 1.

For the RMSE, we observe the same trend as the MAE as shown in Fig. 5b. The proposed model outperforms Baseline 1 with respect to the generalization performance and data efficiency. We can see that our model achieves around 2.2 dBm of RMSE using only 31% of the training data used by Baseline 1. By the definition of RMSE, it penalizes large tails of MSE values. In our dataset, receivers with only NLoS paths have significantly low RSS compared to LoS receivers. Hence, we can see that the proposed model predicts RSS of NLoS areas more robustly than Baseline 1.

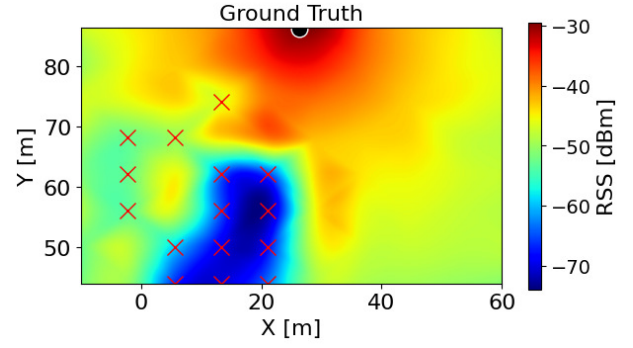
Figure 6 provides a visualization of the predicted RSS maps of the proposed model and Baseline 1. Fig. 6a shows the RGB frame from the camera of BS 1, and Fig. 6b shows the ground truth RSS map, where the red X represents receiver locations with only NLoS paths. We can see that the bus creates a significant NLoS area. This data sample is from the VAL-1 dataset. Hence, this frame is an unseen blockage pattern for both trained models. Figs. 6c and 6d show the predicted RSS maps of the physics-based and Baseline 1 models, respectively. We can see that our model can accurately predict the NLoS



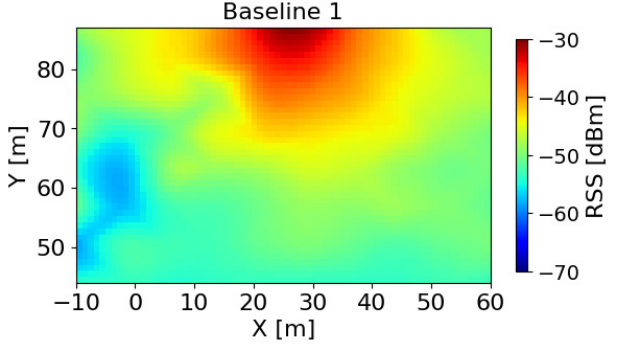
(a) RGB frame captured by BS 1's camera.



(c) Predicted RSS map of the physics-based model

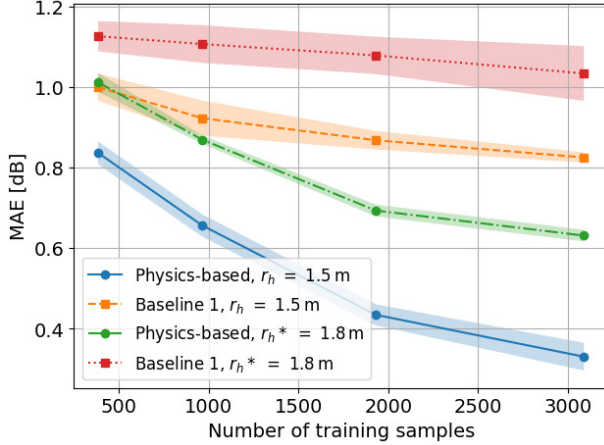


(b) Corresponding true RSS map of BS 1.



(d) Predicted RSS map of the baseline model.

Fig. 6: Visualization of predicted RSS maps of the physics-based and baseline models

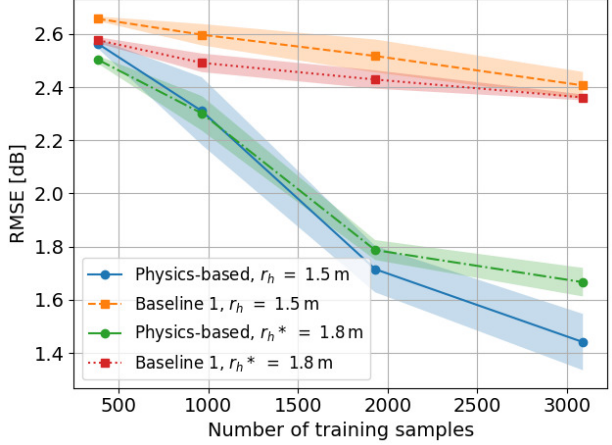


(a) MAE with respect to the amount of training data of BS 1 with unseen receiver height.

Fig. 7: Performance of BS 1 with respect to the amount of training data with unseen receiver height.

area caused by the bus even though this blockage pattern was not shown during the training. Meanwhile, Baseline 1 cannot predict the NLoS region correctly. Although multi-modal data can provide richer information about the environment, vanilla training with MSE loss still learns superficial features rather than learning invariant rules, thereby being sensitive to concept shifts.

Figure 7 shows the performance of BS 1 when receivers with unseen height appear. For the VAL-1 dataset, we set receiver height $r_h = 1.8$ m while we train models with $r_h = 1.5$ m. We mark the cases with the unseen receiver height as $r_h^* = 1.8$ m and the cases with the same receiver



(b) RMSE with respect to the amount of training data of BS 1 with unseen receiver height.

height as $r_h = 1.5$ m for the comparison. We can see that the performance of both the physics-based model and Baseline 1 degrades with the unseen receiver height. However, we can see that the RMSE of the physics-based model is still close to the case when tested with $r_h = 1.5$ m. Hence, we can know that the proposed model still predicts NLoS regions robustly even with unseen receiver heights.

In Figs. 8, we present the performance of our models and baselines on the VAL-1 datasets. The VAL-1 datasets induce both concept and covariate shifts. We can see that our proposed approach is more robust to the domain shifts than the baselines. In Fig. 8, our models improve the MAE and RMSE by 44%

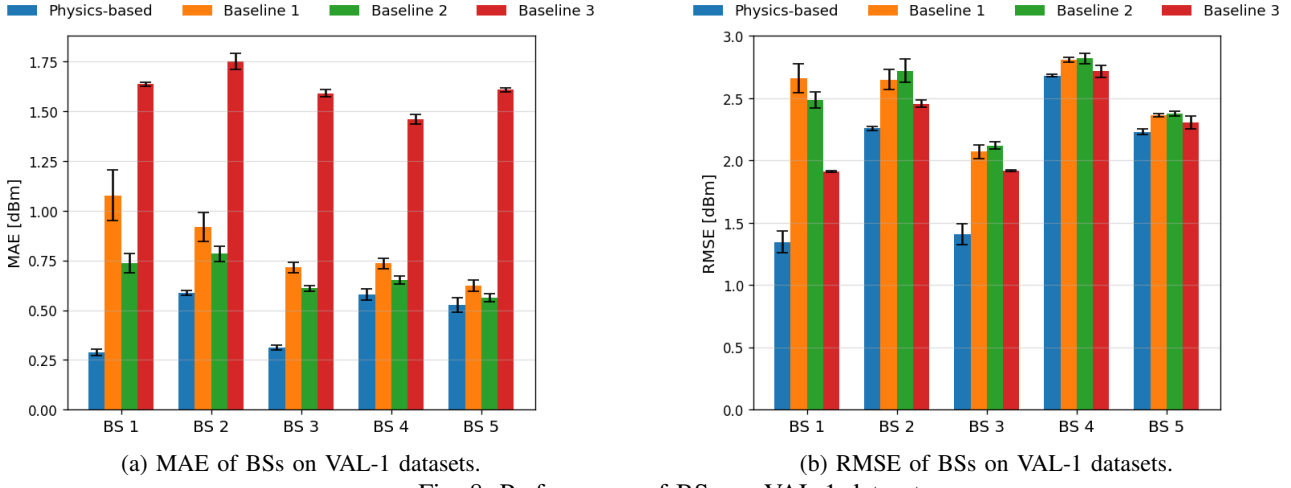


Fig. 8: Performance of BSs on VAL-1 datasets.

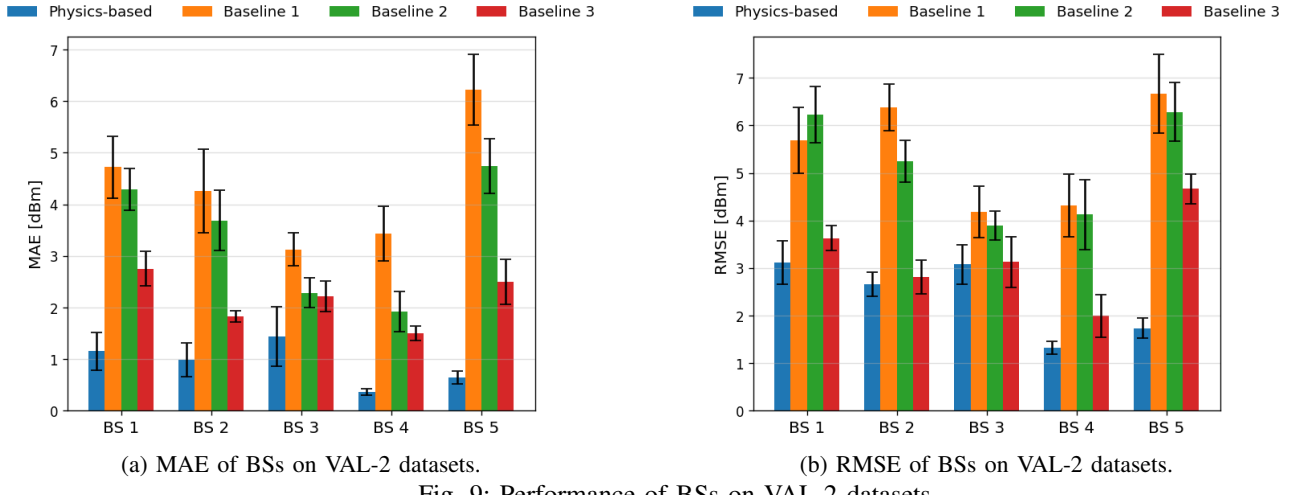


Fig. 9: Performance of BSs on VAL-2 datasets.

and 21%, respectively, compared to those of Baseline 1. For BSs 4 and 5, the performance is lower than that of other BSs because we induced stronger concept shifts by generating unseen large vehicles. Baseline 2 can achieve better MAE than Baseline 1 as it divides the MSE loss function into LoS/NLoS, but its RMSE is similar to that of Baseline 1. This is because Baseline 1 and 2 do not use any physical information for training. Our models improve the MAE and RMSE by 32% and 21%, respectively, compared to those of Baseline 2. Meanwhile, Baseline 3 achieves higher MAE on the VAL-1 than other baselines because it relies on only the 3GPP path loss for LoS points, making it vulnerable to concept shifts. The MAE and RMSE of our models are smaller than those of Baseline 3 by 72% and 12%, respectively.

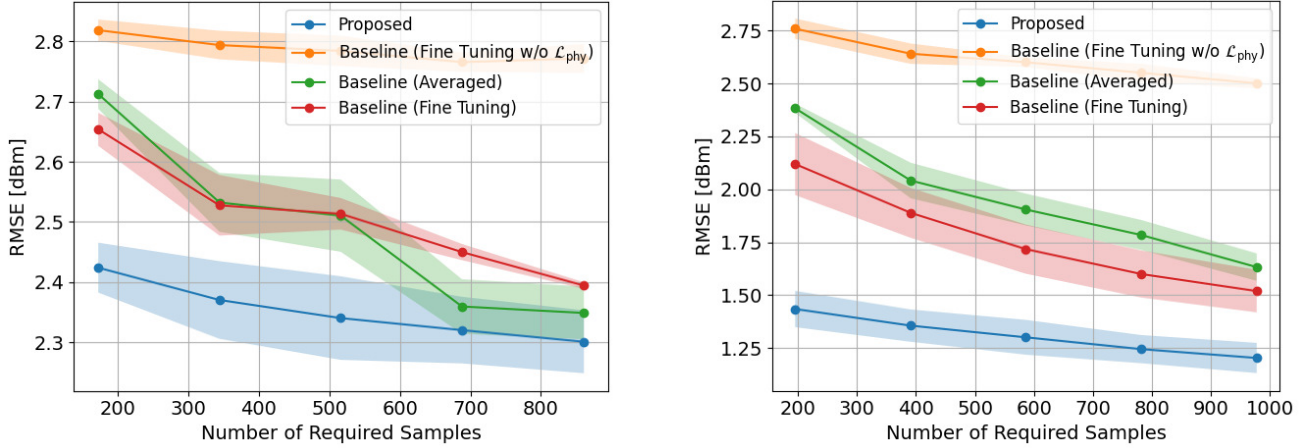
Fig. 9 presents the performance of our models and baselines on the VAL-2 datasets, which induce only covariate shifts. We can see that our approach is significantly more robust to covariate shifts than the baselines. Baselines 1 and 2 are susceptible to covariate shifts because they focus on noise in multi-modal input rather than learning domain-invariant knowledge. The MAE and RMSE of our models are smaller than those of Baseline 1 by 79% and 56%, respectively. For Baseline 2, we can improve the MAE and RMSE by 73% and



Fig. 10: First row: training data of BS 3. Second row: VAL-1 dataset of BS 5

54%, respectively. We can observe that Baseline 3 is more robust to covariate shifts than other baselines because it the 3GPP path loss for LoS points. Hence, covariate shifts does not affect its prediction for LoS points. However, Baseline 3 still shows the degradation for NLoS. Our models can improve the MAE and RMSE by 58% and 27%, respectively, compared to Baseline 3. Hence, physics-based training can improve robustness to both covariate and concept shifts.

Figure 11 presents the performance of the proposed collaborative domain adaptation approach. Here, BSs 4 and 5 observe their VAL-1 datasets after the training. Hence, BSs



(a) RMSE of BS 4 with respect to the amount of data.

Fig. 11: Performance of BS 4 and 5 under domain shifts with the proposed collaborative domain adaptation.

4 and 5 need to adapt to the new environment to recover the performance loss as shown in Fig. 8a. We compare the proposed framework with three baselines. Baseline (Fine Tuning) locally fine-tunes the whole model. Baseline (Averaged) receives model parameters from other agents but, it performs aggregation in a way similar to federated learning’s FedAvg algorithm [31]. Baseline (Fine Tuning w.o. \mathcal{L}_{phy}) locally fine-tunes the entire model without using \mathcal{L}_{phy} . To test the performance of the collaborative domain adaptation approach, we induced similar blockage patterns in the VAL-1 of BSs 4 and 5 to the training data of BSs 1, 2, and 3. A visualization of the example training data of BS 3 and VAL-1 of BS 5 is provided in Fig. 10. Hence, BSs 1, 2, and 3 have useful knowledge that can be helpful to mitigate the domain shift of BS 4 and 5. We can see that our framework outperforms the three baselines with respect to performance and data efficiency. We can observe that the proposed scheme requires significantly less data samples in test-time compared to the baselines. Our scheme needs 25% of data to outperform the Baseline (Fine Tuning). BS 4 and 5 can adapt to the current domain with minimal data samples because they use the knowledge of other agents to mitigate the domain shift. Baseline (Fine Tuning) performs better than other baselines due to the physics-based loss function. However, it needs more data than our scheme because it does not efficiently utilize the knowledge of other agents. Similarly, Baseline (Averaged) averages every model parameters that are not always helpful to mitigate the current domain shift, thereby decreasing the data efficiency.

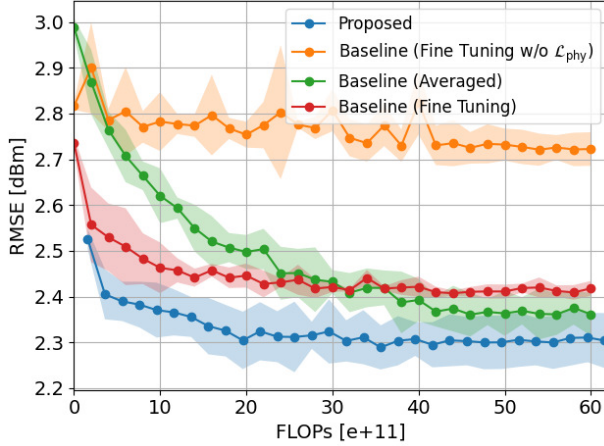
In Fig. 12, we present the learning curves of BS 4 and 5 under the domain shifts used in Fig. 11 with respect to the number of FLOPs. Here, we report FLOPs to measure the compute overhead during the adaptation. We can see that the proposed collaborative domain adaptation converges significantly faster than the baselines with less computation. BS 4 and 5 can initiate their models using the domain similarity-based aggregation. Hence, the proposed aggregation gives a high weight to models that experienced similar domains. Note that our method first retrieves models from other BSs, and does $K - 1$ inferences to calculate the domain similarity as shown in Algorithm. 1, leading to additional computation

and communication overhead. The communication overhead negligible as the model size is 50 Mb and the backhaul often provides throughput of Gbps scale [25]. Calculating domain similarities requires additional forward passes. Hence, in Fig. 12, we can see that the curves of BSs 4 and 5 start later than other baselines that do fine-tuning immediately. However, the baselines show slower convergence due to the lack of enough available data for the adaptation. For Baseline (Averaged), the aggregated model is not helpful to mitigate the current domain shift, and it degrades the performance due to the aggregation of irrelevant models.

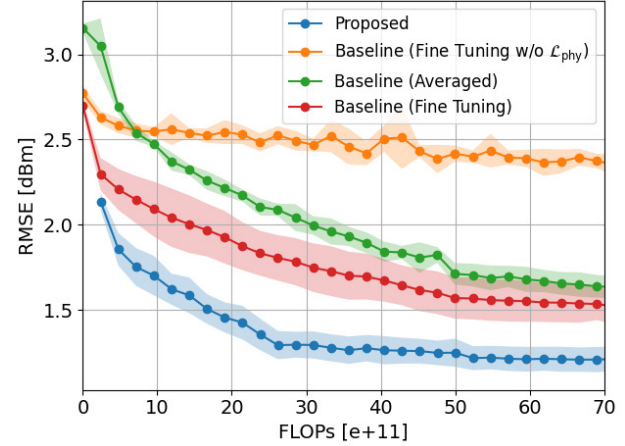
Figure 13 presents the performance of the proposed collaborative domain adaptation with BS 2 using its VAL-2 dataset. To simulate the domain shift, BS2 observes its VAL-2 dataset after the training. To test the performance of the collaborative domain adaptation, we induced the same covariate shift patterns of the VAL-2 to the training datasets of BSs 4 and 5. Hence, BSs 4 and 5 have useful knowledge that guides BS 2 under the domain shift. We can see that our framework outperforms the three baselines with respect to the data efficiency and adaptation speed. In Fig. 13a, we can see that our scheme needs only 40% of data to outperform the Baseline (Fine Tuning). BS 2 shows high data efficiency because it utilizes the knowledge of BSs 4 and 5 to mitigate the current domain shift. Fig. 13 also shows that our method converges faster to better RMSE than other baselines because it starts adaptation by using the knowledge of BSs 4 and 5.

VII. CONCLUSION

In this paper, we have studied the problems of achieving robust generalization to dynamic wireless environments with limited multi-modal data. We have proposed to use physics-based training to improve the data efficiency and robustness to domain shifts. We have presented the theoretical insights on the impact of physics-based training on data efficiency. Then, we have presented the collaborative domain adaptation framework to utilize the knowledge of other BSs to help under-performing BSs under domain shifts to improve the data efficiency and adaptation speed. To this end, we have proposed to measure the domain similarity between each BS

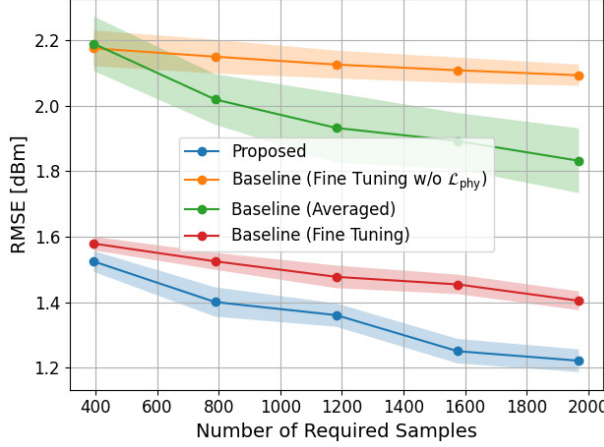


(a) Learning curve of the RMSE of BS 4 under domain shifts.

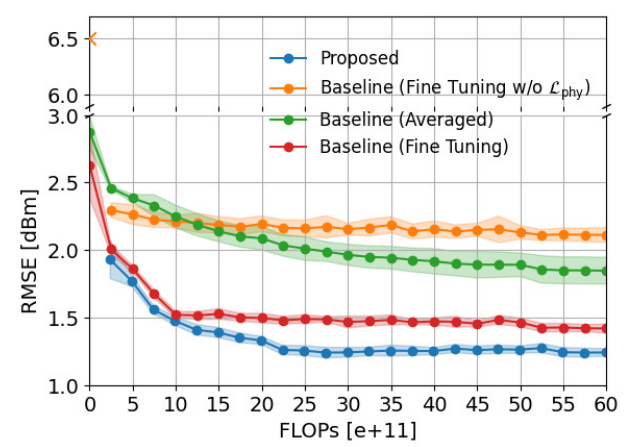


(b) Learning curve of the RMSE of BS 5 under domain shifts.

Fig. 12: Learning curves of BS 4 and 5 under domain shifts with the proposed collaborative domain adaptation.



(a) Learning curve of the RMSE of BS 2 under domain shifts.



(b) Learning curve of the RMSE of BS 2 under domain shifts.

Fig. 13: Learning curves of BS 2 under domain shifts with the proposed collaborative domain adaptation.

to effectively aggregate model parameters of BSs. We have provided one use case of our framework for predicting RSS maps of multiple BSs based on multi-modal data. To validate our framework, we have developed a novel multi-modal dataset that can simulate the proposed use case and induce domain shifts. Simulation results validate the data efficiency, generalization performance, and our theoretical analysis of the proposed frameworks. The proposed algorithms require much less training data than a standard fine-tuning and the baselines to achieve convergence. Moreover, our framework shows stronger generalization to domain shifts under dynamic wireless environments. In essence, this work provides the first systematic study on how to design a learning framework to achieve robust generalization with limited multi-modal data under dynamic wireless environments.

APPENDIX

A. Proof Theorem 1

The proof is inspired by [19]. First, we derive that $\theta \in \Theta(\epsilon_0)$ achieves $\mathcal{L}_{\text{phy}}(\mathbf{Y}, \theta(\mathbf{X})) = 0$ with a certain probability. We assume a set of $\theta \notin \Theta(\epsilon_0)$, where $\Theta(\epsilon_0) = \{\theta \in \Theta : \bar{\mathcal{L}}_{\text{phy}}(\mathbf{Y}, \theta(\mathbf{X})) \leq \epsilon_0\}$. For each data sample \mathbf{X}_i , we define an indicator variable $z_{\text{phy},i} = \mathbb{1}[l_{\text{phy}}(\mathbf{Y}, \theta(\mathbf{X}_i)) = 0]$. Assume that $z_{\text{phy},i}$ follows a Bernoulli distribution such that $p = \mathbb{P}[z_{\text{phy},i} = 1], \forall i$. Then, $\bar{\mathcal{L}}_{\text{phy}}(\mathbf{Y}, \theta(\mathbf{X}))$ can be bounded as follows

$$\bar{\mathcal{L}}_{\text{phy}}(\theta(\mathbf{X})) = \mathbb{E}_{(\mathbf{X}, \mathbf{Y}) \sim \mathbb{P}(\mathbf{X}, \mathbf{Y})}[l_{\text{phy}}(\mathbf{Y}, \theta(\mathbf{X}))] \quad (18)$$

$$= \mathbb{E}_{(\mathbf{X}, \mathbf{Y})}[l_{\text{phy}}(\mathbf{Y}, \theta(\mathbf{X}))]\mathbb{P}[l_{\text{phy}}(\mathbf{Y}, \theta(\mathbf{X})) = 0]$$

$$+ \mathbb{E}_{(\mathbf{X}, \mathbf{Y})}[l_{\text{phy}}(\mathbf{Y}, \theta(\mathbf{X}))]\mathbb{P}[l_{\text{phy}}(\mathbf{Y}, \theta(\mathbf{X})) > 0]$$

$$= (1-p)\mathbb{E}_{(\mathbf{X}, \mathbf{Y}) \sim \mathbb{P}(\mathbf{X}, \mathbf{Y})}[l_{\text{phy}}(\mathbf{Y}, \theta(\mathbf{X}))] \quad (19)$$

$$< (1-p), \quad (20)$$

where the last inequality comes from the assumption that $l_{\text{phy}}(\mathbf{Y}, \theta(\mathbf{X})) \in [0, 1]$. Since $\theta \notin \Theta(\epsilon_0)$, we can bound p as follows

$$p < 1 - \bar{\mathcal{L}}_{\text{phy}}(\mathbf{Y}, \theta(\mathbf{X})) < 1 - \epsilon_0. \quad (21)$$

Then, for $\theta \notin \Theta(\epsilon_0)$ and the number of data samples m , the probability of the empirical loss $\mathcal{L}_{\text{phy}}(\mathbf{Y}, \theta(\mathbf{X}))$ to be zero can be bounded as follows

$$\mathbb{P}[\mathcal{L}_{\text{phy}}(\mathbf{Y}, \theta(\mathbf{X})) = 0] < (1 - \epsilon_0)^m. \quad (22)$$

Then, with probability at least $1 - (1 - \epsilon_0)^m$, only θ with $\mathcal{L}_{\text{phy}}(\mathbf{Y}, \theta(\mathbf{X})) \leq \epsilon_0$ have $\mathcal{L}_{\text{phy}}(\mathbf{Y}, \theta(\mathbf{X})) = 0$. Hence, only $\theta \in \Theta(\epsilon_0)$ achieve $\mathcal{L}_{\text{phy}}(\mathbf{Y}, \theta(\mathbf{X})) = 0$.

Next, we show that only θ with $\bar{\mathcal{L}}_{\text{data}}(\mathbf{Y}, \theta(\mathbf{X})) \leq \epsilon_1$ can achieve $\bar{\mathcal{L}}_{\text{phy}}(\mathbf{Y}, \theta(\mathbf{X})) \leq \epsilon_0$ with a certain probability. We follow similar steps as above. Consider $\theta \in \Theta(\epsilon_0)$ and $\bar{\mathcal{L}}_{\text{data}}(\mathbf{Y}, \theta(\mathbf{X})) > \epsilon_1$. We define $z_{\text{data},i} = \mathbb{1}[l_{\text{data}}(\mathbf{Y}_i, \theta(\mathbf{X}_i)) = 0]$ and assume it follows a Bernoulli distribution such that $p' = \mathbb{P}[z_{\text{data},i} = 1], \forall i$. Then, $\bar{\mathcal{L}}_{\text{data}}(\mathbf{Y}, \theta(\mathbf{X}))$ can be bounded as $\bar{\mathcal{L}}_{\text{data}}(\mathbf{Y}, \theta(\mathbf{X})) < 1 - p'$ as done above. Similarly, we bound p' as follows

$$p' < 1 - \bar{\mathcal{L}}_{\text{data}}(\mathbf{Y}, \theta(\mathbf{X})) < 1 - \epsilon_1. \quad (23)$$

Then, for $\theta \in \Theta(\epsilon_0)$ and $\bar{\mathcal{L}}_{\text{data}}(\mathbf{Y}, \theta(\mathbf{X})) > \epsilon_1$, the probability of $\mathcal{L}_{\text{data}}(\mathbf{Y}, \theta(\mathbf{X}))$ to be zero can be bounded as

$$\mathbb{P}[\mathcal{L}_{\text{data}}(\mathbf{Y}, \theta(\mathbf{X})) = 0] < (1 - \epsilon_1)^m \quad (24)$$

$$< |\Theta(\epsilon_0)|(1 - \epsilon_1)^m \quad (25)$$

$$< |\Theta(\epsilon_0)| \exp(-\epsilon_1 m), \quad (26)$$

where (25) is from the union bound, and the last inequality is from $(1 - x)^y \leq \exp(-xy)$. By bounding (26) with a certain probability $\delta \in (0, 1)$, we can derive the bound of m to satisfy (26) as follows

$$m \geq \frac{1}{\epsilon_1} \left[\ln |\Theta(\epsilon_0)| + \ln \frac{1}{\delta} \right]. \quad (27)$$

Therefore, with probability at least $1 - \delta$, only $\theta \in \Theta(\epsilon_0)$ and $\Theta(\epsilon_1)$ can have $\mathbb{P}[\mathcal{L}_{\text{data}}(\mathbf{Y}, \theta(\mathbf{X})) = 0]$ with the given value of m , thereby proving the theorem.

REFERENCES

- [1] W. Saad, O. Hashash, C. K. Thomas, C. Chaccour, M. Debbah, N. Mandayam, and Z. Han, "Artificial general intelligence (AGI)-native wireless systems: A journey beyond 6G," *Proceedings of the IEEE*, pp. 1–39, 2025.
- [2] Y. M. Park, Y. K. Tun, W. Saad, and C. S. Hong, "Resource-efficient beam prediction in mmwave communications with multimodal realistic simulation framework," *arXiv preprint arXiv:2504.05187*, 2025.
- [3] L. Bai, Z. Huang, M. Sun, X. Cheng, and L. Cui, "Multi-modal intelligent channel modeling: A new modeling paradigm via synesthesia of machines," *IEEE Communications Surveys and Tutorials*, Apr. 2025.
- [4] A. Alkhateeb, G. Charan, T. Osman, A. Hredzak, J. Morais, U. Demirhan, and N. Srinivas, "Deepsense 6G: A large-scale real-world multi-modal sensing and communication dataset," *IEEE Communications Magazine*, vol. 61, no. 9, pp. 122–128, Sep. 2023.
- [5] C. Schuhmann, R. Beaumont, R. Vencu, C. Gordon, R. Wightman, M. Cherti, T. Coombes, A. Katta, C. Mullis, M. Wortsman *et al.*, "Laion-5b: An open large-scale dataset for training next generation image-text models," *Advances in neural information processing systems*, vol. 35, pp. 25 278–25 294, 2022.
- [6] S. Qu, Y. Pan, G. Chen, T. Yao, C. Jiang, and T. Mei, "Modality-agnostic debiasing for single domain generalization," in *Proceedings of the IEEE/CVF Conference on Computer Vision and Pattern Recognition*, 2023, pp. 24 142–24 151.
- [7] X. Zhang, J. Li, W. Chu, R. Xu, Y. Yang, S. Guan, J. Xu, L. Jing, P. Cui *et al.*, "On the out-of-distribution generalization of large multimodal models," in *Proceedings of the Computer Vision and Pattern Recognition Conference*, 2025, pp. 10 315–10 326.
- [8] T. Jiao, Z. Xiao, Y. Xu, C. Ye, Y. Huang, Z. Chen, L. Cai, J. Chang, D. He, Y. Guan *et al.*, "Addressing the curse of scenario and task generalization in AI-6G: A multi-modal paradigm," *IEEE Trans. Wireless Commun.*, Apr. 2025.
- [9] T. Jiao, Z. Xiao, Y. Huang, C. Ye, Y. Feng, L. Cai, J. Chang, F. Liu, Y. Xu, D. He *et al.*, "Ai2mmum: Ai-ai oriented multi-modal universal model leveraging telecom domain large model," *arXiv preprint arXiv:2505.10003*, 2025.
- [10] Z. Chen, Z. Zhang, Z. Xing, R. Li, Z. Yang, R. Jin, C. Huang, Y. Yang, and M. Debbah, "Analogical learning for cross-scenario generalization: Framework and application to intelligent localization," *arXiv preprint arXiv:2504.08811*, 2025.
- [11] S. Liu, Z. Chen, M. Wu, C. Liu, and L. Chen, "Wisr: Wireless domain generalization based on style randomization," *IEEE Trans. Mobile Comput.*, vol. 23, no. 5, pp. 4520–4532, May 2024.
- [12] S. Liu, Z. Chen, M. Wu, H. Wang, B. Xing, and L. Chen, "Generalizing wireless cross-multiple-factor gesture recognition to unseen domains," *IEEE Trans. Mobile Comput.*, vol. 23, no. 5, pp. 5083–5096, May 2024.
- [13] Y. Zhang, Q. Li, H. Liu, L. Yang, and J. Yang, "Domain generalization for cross-receiver radio frequency fingerprint identification," *IEEE Internet Things J.*, vol. 12, no. 5, pp. 5207–5218, Mar. 2025.
- [14] A. Seretis and C. D. Sarris, "Toward physics-based generalizable convolutional neural network models for indoor propagation," *IEEE Trans. Antennas Propag.*, vol. 70, no. 6, pp. 4112–4126, 2022.
- [15] T. Li, H. Lei, H. Guo, M. Yin, Y. Hu, Q. Zhu, and S. Rangan, "Digital twin-enhanced wireless indoor navigation: Achieving efficient environment sensing with zero-shot reinforcement learning," *IEEE Open Journal of the Communications Society*, Mar. 2025.
- [16] Y. Zheng, J. Wang, X. Li, J. Li, and S. Liu, "Cell-level rsrp estimation with the image-to-image wireless propagation model based on measured data," *IEEE Trans. Cogn. Commun. Netw.*, vol. 9, no. 6, pp. 1412–1423, Dec. 2023.
- [17] Z. Li, M. Chen, G. Li, X. Lin, and Y. Liu, "Map-driven mmwave link quality prediction with spatial-temporal mobility awareness," *IEEE Trans. Mobile Comput.*, Dec. 2024.
- [18] A. Dosovitskiy, G. Ros, F. Codevilla, A. Lopez, and V. Koltun, "Carla: An open urban driving simulator," in *Conference on robot learning*, 2017, pp. 1–16.
- [19] S. Garg and Y. Liang, "Functional regularization for representation learning: A unified theoretical perspective," *Advances in Neural Information Processing Systems*, vol. 33, pp. 17 187–17 199, 2020.
- [20] M. Kim, W. Saad, M. Debbah, and C. S. Hong, "Spaf: Communication-efficient federated learning with sparse models and low computational overhead," *Advances in Neural Information Processing Systems*, vol. 37, pp. 86 500–86 527, 2024.
- [21] J. Tian, Y.-C. Hsu, Y. Shen, H. Jin, and Z. Kira, "Exploring covariate and concept shift for out-of-distribution detection," in *NeurIPS 2021 Workshop on Distribution Shifts: Connecting Methods and Applications*, 2021.
- [22] S. Jaekel, L. Raschkowski, S. Wu, L. Thiele, and W. Keusgen, "An explicit ground reflection model for mm-wave channels," in *Proc. IEEE Wireless Commun. and Networking Conf.*, San Francisco, CA, USA, May 2017, pp. 1–5.
- [23] "3gpp tr 38.901 v14.2.0, "study on channel model for frequencies from 0.5 to 100 ghz," 2019.
- [24] U.S. Department of Transportation. Advanced messaging concept development: Basic safety message. [Online]. Available: https://data.transportation.gov/Automobiles/Advanced-Messaging-Concept-Development-Basic-Safety-eezi-v4pm/about_data
- [25] B. Tezergil and E. Onur, "Wireless backhaul in 5g and beyond: Issues, challenges and opportunities," *IEEE communications surveys and tutorials*, vol. 24, no. 4, pp. 2579–2632, 2022.
- [26] C. Conlan, "The blender python api," *Precision 3D Modeling and Add*, 2017.
- [27] A. Ali, N. González-Prelcic, and A. Ghosh, "Passive radar at the roadside unit to configure millimeter wave vehicle-to-infrastructure links," *IEEE Trans. Veh. Technol.*, vol. 69, no. 12, pp. 14 903–14 917, Dec. 2020.
- [28] W. Xu, F. Gao, X. Tao, J. Zhang, and A. Alkhateeb, "Computer vision aided mmwave beam alignment in v2x communications," *IEEE Trans. Wireless Commun.*, vol. 22, no. 4, pp. 2699–2714, Apr. 2022.
- [29] A. Narayanan, E. Ramadan, R. Mehta, X. Hu, Q. Liu, R. A. Fezeu, U. K. Dayalan, S. Verma, P. Ji, T. Li *et al.*, "Lumos5g: Mapping and predicting commercial mmwave 5g throughput," in *Proceedings of the ACM internet measurement conference*, 2020, pp. 176–193.
- [30] H. Yao, Y. Wang, L. Zhang, J. Y. Zou, and C. Finn, "C-mixup: Improving generalization in regression," *Advances in neural information processing systems*, vol. 35, pp. 3361–3376, 2022.
- [31] M. Kim, W. Saad, M. Mozaffari, and M. Debbah, "Green, quantized federated learning over wireless networks: An energy-efficient design," *IEEE Trans. Wireless Commun.*, vol. 23, no. 2, pp. 1386–1402, Feb. 2024.